Proceedings of the Combustion Institute 41 (2025) 105854

Contents lists available at ScienceDirect

Proceedings of the Combustion Institute

journal homepage: www.elsevier.com/locate/proci

Experimental and numerical investigation of non-premixed ammonia flames stabilized on a heated slot burner

Daniel Kretzler [a,*], Rishabh Puri [a], Björn Stelzner [a], Thorsten Zirwes [b], Fabian P. Hagen [a], Oliver T. Stein [a], Dimosthenis Trimis [a]

[a] Karlsruhe Institute of Technology (KIT), Engler-Bunte-Institute, Combustion Technology, Engler-Bunte Ring 7, D-76131 Karlsruhe, Germany
[b] University of Stuttgart, Institute for Reactive Flows, Pfaffenwaldring 31, D-70569 Stuttgart, Germany

ARTICLE INFO

Keywords:
Ammonia combustion
Non-premixed combustion
NO_x emissions

ABSTRACT

In this study, non-premixed laminar ammonia/air flames are investigated using a custom-designed heated slot burner developed at KIT. This innovative setup enables investigations into ammonia decomposition and pollutant formation processes through in-situ diagnostics, numerical simulations, and global performance analyses, providing a unique dataset. Experiments are conducted at three oven temperatures (T = 1073 K, 1123 K, and 1173 K) and two thermal loads (0.2 and 0.6 kW) at a global equivalence ratio of $\Phi = 1$. Inlet temperatures, as well as qualitative insights into NH*, NH_2*, and OH* along the flame are obtained using thermocouples and emission spectroscopy. To assess global combustion characteristics, gas analyzers measure exhaust species, including NO, NO_2, N_2O, NH_3, and O_2. The experimental setup is reconstructed in two dimensions for numerical simulations using an in-house OpenFOAM solver. Flame and emission characteristics are investigated for different operating conditions and chemical mechanisms. While experiments and simulations agree well regarding flame length, flame stability, and chemiluminescence profiles, some deviations in exhaust gas emissions remain. These are attributed to experimental uncertainty from the assumption of flow symmetry, boundary conditions, and uncertainty due to the choice of chemical reaction mechanism at elevated temperatures. Emissions are strongly influenced by oven temperature and flow velocity, with lowest NH_3, N_2O, and NO_x levels observed at high oven temperatures. The non-premixed configuration achieves NO_x emissions down to 335 ppmv at $\Phi = 1$, significantly below values from premixed combustion, which typically exceed several thousand ppmv. Pathway analysis reveals that the investigated reaction mechanisms predict routes with different relative contributions to NO production, but provide similar trends for NO consumption. The results highlight the suitability of the platform for systematic ammonia combustion studies and the potential of non-premixed strategies for NO_x mitigation.

1. Introduction

Ammonia is an emerging fuel with significant potential for zero-carbon energy storage, transport, and conversion. Its excellent ability to store and transport hydrogen makes it an attractive candidate for renewable energy applications [1]. Recently, the direct use of ammonia as fuel has come into focus due to its potential for improved overall efficiency compared to utilizing ammonia as a hydrogen carrier and cracking it into hydrogen prior to combustion. Therefore, from an efficiency standpoint, the direct combustion of ammonia presents a more favorable alternative [2]. However, the combustion of ammonia poses several challenges. The low reactivity and corresponding low flame speed of ammonia make it challenging to achieve stable combustion. In addition, combustion is often accompanied by elevated emissions of pollutants such as unburned ammonia and nitrogen oxides. In particular, lean conditions tend to produce high levels of nitrogen oxides, whereas under rich conditions, unburned ammonia becomes the dominant pollutant. Additionally, nitrous oxide emissions typically occur at concentrations three orders of magnitude lower than NO_x emissions [3,4]. However, given its substantial climate impact, having a 20-year global warming potential 273 times that of CO_2, N_2O should also be taken into account [5]. Despite its lower concentrations, its contribution remains significant and should be minimized, considering potential regulatory restrictions [6,7]. Therefore, the growing interest in the direct energetic use of ammonia necessitates the development of an appropriate combustion technology for low-emission conversion.

* Corresponding author.
E-mail address: daniel.kretzler@kit.edu (D. Kretzler).

https://doi.org/10.1016/j.proci.2025.105854
Received 2 May 2025; Accepted 4 September 2025
Available online 24 September 2025

To achieve flame stability, swirl burners are commonly investigated for ammonia combustion [1,8]. The stability of ammonia flames can also be significantly enhanced by preheating of the reactants or hydrogen addition [1,9]. While unburned ammonia remains a concern, hydrogen addition promotes NO_x and N_2O formation across different equivalence ratios. In comparison, operating under fuel-lean conditions causes a much stronger increase in these emissions, making the influence of hydrogen addition relatively minor in this context [4]. Overall, a fundamental trade-off exists between ammonia slip for fuel-rich and NO_x emissions for fuel-lean conditions [10]. NO_x emissions are a significant challenge due to the fuel-bound nitrogen in ammonia combustion. In the case of pure ammonia-air combustion, the Zel'dovich mechanism is not the primary pathway of NO_x formation [1,3]. Recently, non-premixed ammonia combustion has been demonstrated as a promising concept for reducing NO_x emissions. Zhang et al. [11] demonstrated the non-premixed operation of a swirl burner with 30 % H_2 addition at Φ = 1 with NO_x < 30 ppmv and unburned NH_3 < 1500 ppmv, both normalized to 15 % O_2. Chen et al. [12] also reported NO_x and NH_3 emissions below 100 ppmv at preheating temperatures above 640 K. In addition, combustion within porous media presents a promising approach for improving flame stabilization and reducing pollutant emissions. In these burners, heat recirculation between the hot combustion zone and the incoming cold gases preheats the reactants, improving combustion efficiency. This occurs due to gas and solid phase interaction by thermal radiation, convection, and heat conduction, greatly increasing the effective flame speed [13,14]. Low-emission combustion can be achieved by optimizing boundary conditions, including thermal properties and flow control [14,15]. To minimize NH_3 slip, high temperatures, lean conditions, and complete mixing are essential [16,17].

Addressing these challenges, namely high NO_x emissions, unburned ammonia, and limited flame stability, requires an improved understanding of the complex combustion behavior of ammonia to ensure its reliable use in large-scale applications [3]. Slot burners are well-suited for studying specific combustion characteristics due to their tailored design and optical access. For instance, Murai et al. [18] investigated the effect of oxygen enrichment on the laminar flame speed during premixed ammonia combustion in a slot burner. For further diagnostics, emission spectroscopy serves as a valuable tool for obtaining non-intrusive, spatially-resolved insights into flame chemistry. It has been widely applied in studies on ammonia flames, allowing for qualitative spatial analysis of excited species within the flame. Recently, Issayev et al. [19] utilized chemiluminescence imaging to investigate NH* and OH* in non-premixed ammonia-hydrogen counterflow flames across a hydrogen mole fraction range of x_{H_2} = 10%–90%, comparing their results with the mechanism proposed by Konnov [20,21]. Similarly, Pugh et al. [22] employed line-of-sight integrated imaging of NH*, NH_2*, and OH* in turbulent diffusion flames. Their findings indicate chemiluminescence measurements provide valuable insights into intermediate reaction pathways.

This study investigates non-premixed NH_3 flames in a slot burner under various operating conditions to provide fundamental insights leading to low-emission ammonia combustion. The burner enables sufficient preheating for flame stabilization and establishes a quasi-2D configuration, which simplifies numerical modeling. Experimental data are compared to 2D simulations of the reacting flow, including a systematic comparison of reaction mechanisms. Residence times and boundary temperatures are varied to analyze their impact on flame stability, length, in-flame species, and exhaust gas composition. The dataset offers a valuable basis for mechanism validation and the development of low-emission combustion systems.

2. Methods

2.1. Experimental setup

The experiments are conducted using a custom-designed heated slot burner, developed at KIT, see Fig. 1. This novel setup provides optical access to study stabilized (quasi-)2D non-premixed laminar ammonia flames. The base of the burner consists of welded stainless steel plates forming a hollow chamber, into which fuel and air are fed through two separate pipes, each with an inner diameter of 10 mm. A splitter plate (silicon nitride, thickness 1 mm, Xtra) divides the hollow chamber into two sections for non-premixed operation. The widths of the fuel and air chambers are 1.97 mm and 7.03 mm, respectively, ensuring an equivalent flow velocity without shear at stoichiometric combustion conditions (Φ = 1). To achieve a homogeneous flow profile, a flow straightener consisting of two laser-cut stainless steel meshes (mesh sizes 0.3 and 0.2 mm, wire diameters 0.2 and 0.125 mm, Dorstener Drahtwerke) is installed at the top of the base. The burner design is significantly wider (150 mm) than the measuring region in the center (20 mm) to minimize the influence of the edges on the flame and flow profile. The outlet of the hollow chamber is connected to a rectangular quartz tube (d_i = 10 mm, w_i = 150 mm, h = 250 mm, wall thickness = 2 mm, QGH), which encloses the flame. The quartz tube is uniformly heated along its entire length by an oven with a maximum power output of 2 kW and a peak operating temperature of 1500 K, enabling flame stabilization under well-defined boundary conditions. The oven has a total vertical height of 280 mm and an inner spanwise cross section of 300 x 110 mm. Thermal insulation is provided by 100 mm thick vacuum-formed ceramic fiber (ASW). The oven is heated by a CrFeAl heating wire (diameter 1.5 mm, total length 30.8 m) wound into horizontal coils (inner diameter 10 mm) along its height, providing uniform temperature distribution. A 4 mm thick quartz window is embedded vertically at the oven center for optical access. Its diameter (30 mm) is small relative to the oven (300 mm), reducing temperature inhomogeneities. The oven temperature is monitored by two thermocouples. Details on their positioning and the temperature control system are provided in Section 2.2.

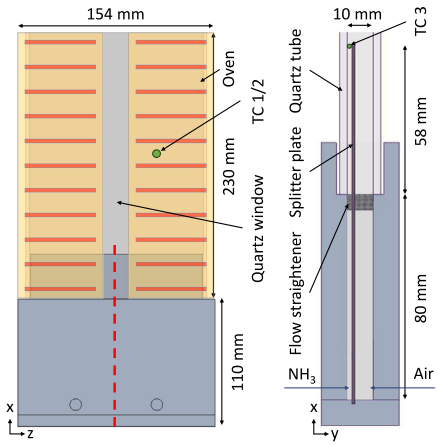

Fig. 1. Illustration of the slot burner and the heating oven environment (left, oven shown schematically for clarity), and enlarged cross-sectional view (right) indicated by the red dashed line on the left. TC: thermocouple.

2.2. Instrumentation and measurements

The gas flow rates are controlled using mass flow controllers (MFCs, Bronkhorst) with a relative accuracy better than 0.5%. For fuel gases, pure NH_3 (Air Liquide) with a purity better than 99.98% is used. To ensure continuous gas flow, the liquefied NH_3 cylinders are kept at room temperature using a heating system. An RGB CMOS camera (Blue Fox 3-2071aC, Matrix Vision) is used to visualize the flame luminosity and its position. For flame diagnostics, temperature measurements, exhaust gas analysis, and emission spectroscopy are conducted. Temperature measurements are performed to determine the boundary conditions for combustion using three type S thermocouples (see Fig. 1). To

Table 1
Characteristic wavelengths of the investigated radicals and their corresponding electronic transitions.

Species	λ (nm)	Transition	Ref.
OH*	309	$A^2\Sigma^+ \rightarrow X^2\Pi$	[20]
NH*	336	$A^3\Pi \rightarrow X^3\Sigma^-$	[20]
NH_2*	630	$A^2A_1 \rightarrow X^2B_1$	[22]

prevent catalytic effects of the platinum, the thermocouples are coated with an adhesive ceramic compound (Resbond 904, Cotronics). Two thermocouples (TC 1 and 2) are placed symmetrically at mid-height on opposite sides of the oven, 10 mm from the slot burner and 40 mm from the inner wall, each laterally offset by 20 mm from the quartz window. The thermocouples are assumed to be in radiative equilibrium with the surrounding heating coils. They redundantly monitor the oven temperature, thereby establishing the ambient temperature for flame stabilization. Temperature control is achieved via a PID temperature controller (Eurotherm 2132), which maintains the oven at the specified operating point. The third thermocouple (TC 3), positioned at the end of the splitter plate within the flame channel, is used to measure the inlet temperature of the reactants. Inlet temperature measurements over time are used to evaluate burner stability, with a stability indicator for all experiments defined as a temperature deviation of 0.5 K/min, starting after ignition, supported by a pilot flame at the outlet.

To measure the exhaust gas species, a sampling probe with a diameter of 10 mm and heated tubing to the gas analyzers is positioned directly at the burner outlet, centered on the rectangular quartz glass tube. Gas analyzers (ABB) are used to detect N_2O (0–500 ppmv, Uras 26) in the dry gas phase, while NH_3 (0–2000 ppmv, Limas21), NO (0-10000 ppmv, Limas21), and NO_2 (0–1000 ppmv, Limas21) are measured in the wet gas phase to avoid losses due to condensation. The measurement uncertainties are below 1.5% and the response times are less than 4 s. Signal acquisition relies on a NI-9208 current-input module housed in a NI-DAQ-9179 chassis. All data are averaged over at least 2 min after flame stabilization. To ensure comparable data, all species are normalized to 15 % O_2, in accordance with standard practice for gas turbines [23]:

$$X_{i,15\%O_2} = X_i \frac{X_{O_2,air} - X_{O_2,ref}}{X_{O_2,air} - X_{O_2,meas}} \quad (1)$$

with $X_{O_2,air} = 20.95\%$ and $X_{O_2,ref} = 15.0\%$.

Non-intrusive, spatially-resolved emission spectra are recorded to investigate the in-flame chemical species, with measurements taken at varying heights above the splitter plate. These spectra are captured using a grating spectrometer (Princeton HRS-300, 20 µm Slit, 1200 grids/mm, Blaze 300 nm) coupled to an intensified CMOS camera (IRO X, LaVision; sCMOS CLHS, LaVision). The imaging optics provide a spatial resolution in the sub-millimeter scale. The species quantification is carried out using the characteristic emission wavelengths of excited species, which are listed in Table 1. Background noise is removed by recording dark shots at each measurement point (defined by the height above the splitter plate) in the absence of a flame. The chemiluminescence images are then corrected by subtracting the corresponding dark shots, thereby eliminating background radiation from the oven and surroundings. To enable accurate evaluation of individual emission peaks, a baseline correction is applied during data analysis. The analysis is performed in MATLAB [24] using an asymmetric least squares (ALS) fitting method. Subtracting the fitted baseline from the raw data isolates the emission peaks by removing the underlying flame background.

2.3. Investigated configurations

Experiments are conducted at three different oven temperatures (T = 1073 K, 1123 K and 1173 K) and two thermal loads (0.2 and 0.6 kW) at a global equivalence ratio of $\Phi = 1$. In comparison to the 0.2 kW power setting, the inflow velocity increases by factor of three at 0.6 kW. Table 2 shows that as thermal load – and consequently flow velocity – increases, the steady-state inlet temperature of the reactants decreases. This reduction is attributed to the shorter residence time in the heated section of the burner.

Table 2
Measured temperatures of the oven and the inlet at the height of the slot. Inlet velocity of the reactants at standard temperature and pressure (STP) at different thermal loads.

P (kW)	T_{oven} (K)	T_{in} (K)	u_{in} (cm s^{-1}, STP)
0.2	1073	1048	4.34
0.2	1123	1087	4.34
0.2	1173	1130	4.34
0.6	1073	960	13.02
0.6	1123	999	13.02
0.6	1173	1045	13.02

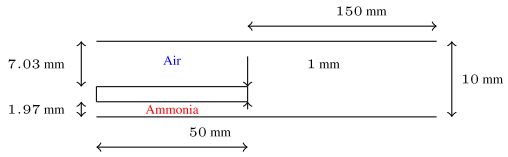

Fig. 2. Burner schematic used for 2D simulations.

2.4. 2D-simulations: numerical model

Simulations were performed using an in-house OpenFOAM-based transient reacting flow solver. The governing equations described in [25] are solved in their variable-density formulation using the finite-volume method. Finite rate chemistry and gas transport properties are calculated by Cantera [26] which is coupled with the solver. Gas diffusion is modeled by the mixture-averaged model using the Hirschfelder-Curtiss approximation [27]. To evaluate results from various state-of-the-art kinetic mechanisms, exhaust gas emissions are predicted using the ammonia reaction mechanisms developed by Konnov [20,21], Stagni et al. [28] and Zhang et al. [29], with the latter also referred to as the KAUST mechanism. In addition, the Konnov mechanism comprehensively accounts for the excited species described in Section 2.2 and is therefore used to predict the measured intensity profiles. The burner schematic used for the simulations is shown in Fig. 2 and the main burner operating parameters are described in Table 2. A fixed-value boundary condition is imposed at the inlet ($x = 0$ mm) for both velocity and temperature. The inlet velocity u_{in} is calculated based on the values of T_{in} and $u_{in,STP}$ listed in Table 2. The burner walls and the splitter plate are assumed to have constant wall temperatures, with $T_{wall} = T_{split} = T_{oven}$ applied uniformly along the entire length of the domain. Heat transfer between the gas phase and the solid boundaries is fully resolved. At the burner outlet, adiabatic boundary conditions are applied. The grid size for the reaction zone is taken as one tenth of the thickness of a 1D freely propagating, premixed stoichiometric NH_3/air flame calculated using Cantera.

3. Results and discussion

3.1. Flame properties

Fig. 3 illustrates that with increasing thermal load and flow velocity, there is a significant increase in both the length and intensity of flame luminosity, indicating a modified ignition and reaction zone. This observation is consistent with theoretical predictions, which suggest that an increased flow velocity leads to delayed ignition and a more extended reaction zone. The visible flame luminosity is primarily

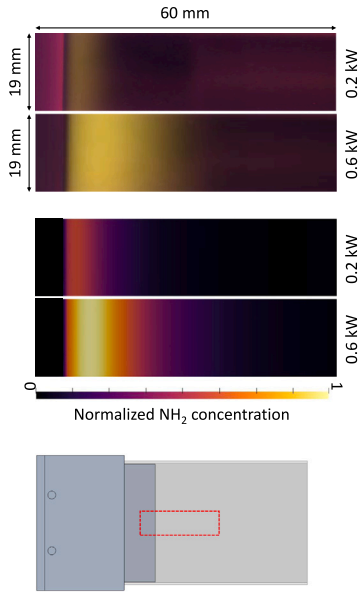

Fig. 3. Exemplary images (top) of various studied ammonia-air flames at an oven temperature of 1073 K, corresponding predicted NH_2 concentration profiles (middle), and the measurement location, marked by a red rectangle (bottom).

attributed to NH_2* emissions [30]. Captured flame images exhibit a good qualitative agreement with the predicted NH_2 concentration profiles, indicating that the reacting flow solver captures the major flame characteristics.

3.2. Emission spectra

Chemiluminescence diagnostics of radical-specific emissions (NH_2*, NH*, and OH*) provide deep insights into the flame characteristics of ammonia combustion. Exemplary emission spectra, along with the corresponding wavelengths of the species listed in Table 1, are shown in Fig. 4. A baseline correction is applied for data analysis, allowing for a precise evaluation of the single emission peaks. To analyze the distribution of individual species within the flame profile, specific wavelength intervals are carefully selected and integrated to refine the data. The resulting intensity measurements are then normalized by the maximum value among all measured operating conditions for each species and plotted against the height above the splitter plate H. Simultaneously, numerical simulations are performed using the Konnov mechanism, which comprehensively accounts for all relevant excited species. The computed mole fractions of these species are normalized and presented alongside the experimental data, allowing for a qualitative comparison of the profiles. Fig. 5 shows that the experimental chemiluminescence profiles are in good agreement with the numerical simulations in terms of both shape and normalized intensity especially at $P = 0.6$ kW. Simulations reliably predict the effects of variation in temperature and thermal load, as well as the regions where chemiluminescence emissions from NH_2*, NH*, and OH* are observed. Both normalized intensity and concentration increase with rising temperature or thermal load. Moreover, an increase in thermal power causes the peak intensity region to shift downstream. These effects can be attributed to diffusion-governed non-premixed combustion. In the absence of shear between fuel and oxidizer, relative heat loss, temperature, and combustion intensity are expected to scale approximately with inflow velocity and thermal load. In addition, at higher velocities, the reduced residence time is expected to cause a downstream shift and lengthening of the reaction zone. In general, all measured chemiluminescence peaks appear slightly further downstream than predicted in the simulations. These small discrepancies may be attributed to limitations of the reaction mechanisms or to stronger heat losses in the experiment than those considered in the model. Based on the flame image in Fig. 3, a distinct flame lift-off cannot be clearly identified. Furthermore, the measured NH_2* and NH* profiles at a thermal load of 0.2 kW appear broader and exhibit higher peak magnitudes compared to the simulations, whereas OH* shows reasonable agreement in magnitude (see Fig. 5). These differences might be related to deviations in the dominant reaction pathways predicted by the mechanisms. For instance, the increased relative intensity of NH_2* emissions observed at a thermal load of 0.2 kW may indicate a more pronounced NH_3 decomposition (NH_3 + OH ↔ NH_2 + H_2O) or an enhanced NO_x reduction (NH_2 + NO ↔ NNH + OH) [22].

3.3. Exhaust gas measurements

Analysis of the exhaust gas composition reveals significant sensitivity of the concentrations of NO_x, NH_3, and N_2O to thermal load and oven temperature. The present section discusses the experimental trends first, followed by the numerical predictions. Fig. 6 shows that measured N_2O emissions decrease with increasing temperature and power, reaching a minimum concentration of 3 ppmv at 0.6 kW and an oven temperature of 1173 K. In addition, measured NH_3 emissions at 0.2 kW decrease with rising temperature, reaching a minimum of 4 ppmv at 1173 K. In contrast, at the same oven temperature (1173 K) but at a higher thermal load (0.6 kW), measured NH_3 emissions are approximately three orders of magnitude higher (1600 ppmv) and show considerably less temperature dependence. For measured NO_x, low-power conditions result in increasing emissions with temperature, reaching a maximum concentration of 4700 ppmv, while at the higher thermal load (0.6 kW) the opposite trend is observed, with NO_x emissions decreasing to a minimum of 335 ppmv. For comparison, typical NO_x levels in premixed NH_3/air combustion at $\Phi = 1$ often exceed several thousand ppmv [3,9]. Subsequently, the numerical results are analyzed and compared with the experimental data. Even though flame location and intensity profiles of chemically excited species match closely between measurements and simulation, there are considerable differences in magnitude and trends of the pollutant emission predictions. Additionally, results were found to depend strongly on the choice of reaction mechanism. Calculated N_2O emissions follow a trend consistent with the experimental data; nevertheless, the emission levels are underestimated, particularly with the KAUST mechanism. NH_3 emissions show a similar trend with respect to the oven temperature and are in good agreement in the case of 0.2 kW, particularly for the Stagni mechanism. However, the values for 0.6 kW thermal load differ by several orders of magnitude. Regarding NO_x, the predicted emissions strongly vary as a function of oven temperature, thermal load, and employed ammonia chemistry. Overall, it is evident that accurately capturing NH_3 chemistry still remains a challenge and that the chemical kinetics play a significant role in the resulting emission characteristics. It is also important to note that the experiments are conducted under non-premixed and strongly preheated conditions, whereas the employed reaction mechanisms have primarily been validated for different combustion regimes. In particular, there is insufficient validation data for non-premixed conditions or elevated temperatures. Regarding NH_3 and N_2O emissions, the mechanisms developed by Stagni et al. and Konnov show similar trends, whereas all mechanisms differ for NO_x emissions for the 0.2 kW case. In addition, simplifications in the numerical model and the experimental setup may introduce uncertainties and affect the quantitative evaluation of the results. Specifically, emission measurements rely on exhaust gas sampling at a single outlet location (see Section 2.2), assuming quasi two-dimensional flow symmetry. Simulations indicate that at the outlet the flow is compositionally uniform and reactions are essentially completed. While this 2D assumption simplifies the experimental implementation and facilitates data interpretation, it may lead to inaccuracies in the presence of asymmetric

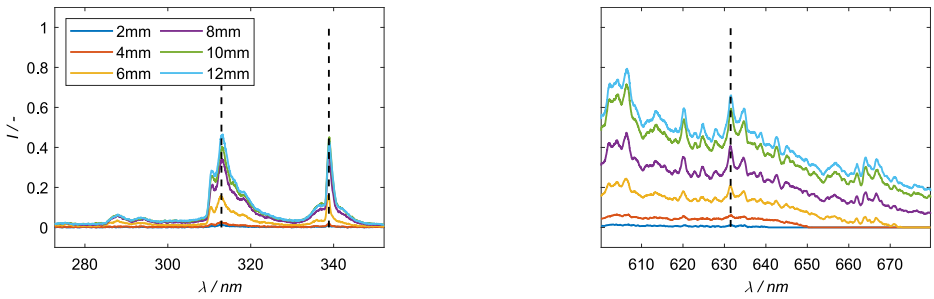

Fig. 4. Exemplary, spatially-resolved spectra at $T = 1073$ K and $P = 0.6$ kW, for the species OH* (309 nm) and NH* (336 nm) in the UV region (left) and NH_2* (630 nm) in the visible region (right), with the normalized intensity of each spectrum plotted against the detection wavelength as a function of height H above the splitter plate (colors).

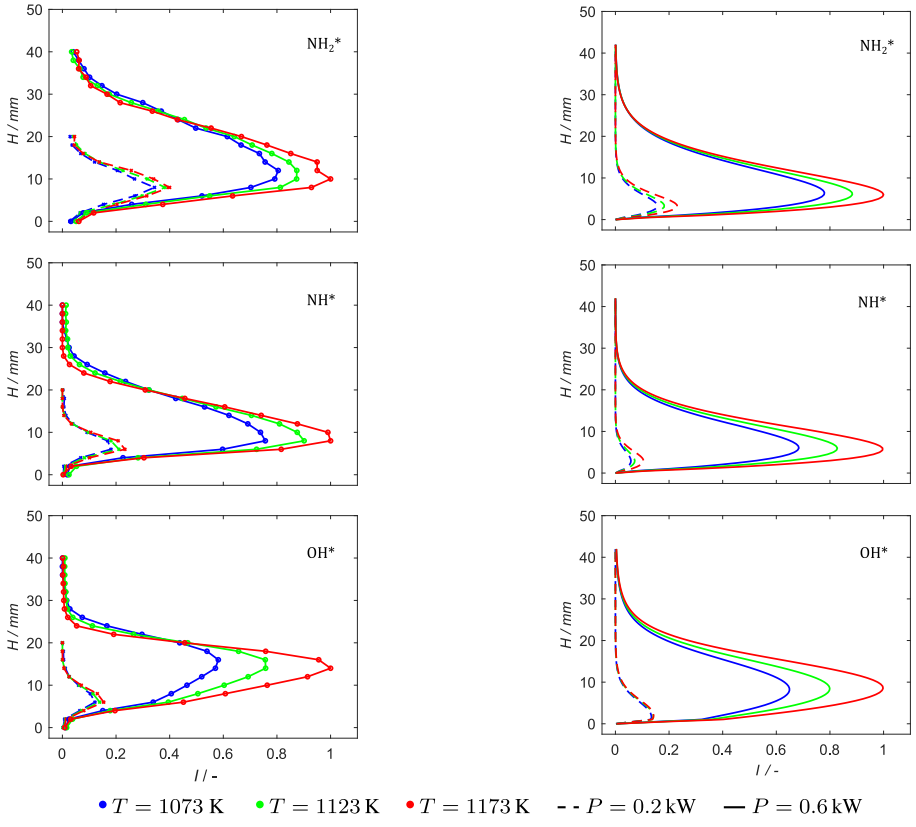

Fig. 5. Normalized intensity profiles of NH_2*, NH*, and OH* from the measurements (left) and simulations (right, Konnov mechanism [20]), shown as a function of the height above the splitter plate at different oven temperatures and power levels (see legend for details).

flame structures. Since the experiments are conducted on a laboratory scale, even minor disturbances in the boundary conditions or burner alignment may affect the flow field and flame structure, potentially favoring unburned species slip and violating the 2D assumption. To reduce associated uncertainties, future investigations may benefit from spatially-resolved gas sampling to better capture potential spanwise inhomogeneities. Moreover, the choice of temperature boundary conditions in the simulation may influence the quantitative agreement with the experimental data. Refining these assumptions in future studies could improve the predictive accuracy of the model.

3.4. Pollutant formation analysis

To address one of the major uncertainties discussed in the previous section, a chemical analysis of the pollutant formation is conducted. NO_x predictions for $P = 0.6$ kW in Fig. 6 (bottom right) show good agreement with the experimental results for $T_{oven} = 1173$ K, whereas considerable differences are observed among the different reaction mechanisms and the experimental results for $T_{oven} = 1073$ K. To explain these differences, the NO formation and reaction pathways are investigated. The production ($\dot{\omega} > 0$) and consumption ($\dot{\omega} < 0$) rates of H_2 and NO in the reaction zone are plotted as contours in Fig. 7. The H_2 consumption zone coincides with the production zone of NO and vice versa. H_2 is produced from NH_3 on the rich side and diffuses to the lean side, where it is consumed. Simultaneously, the presence of O_2 on the lean side facilitates NO production, while NO is reduced on the rich side.

Pathways of atomic N in the production and consumption zones of NO for the Konnov and Stagni mechanisms are shown in Figs. S1 and S2 in the supplementary material. There, atomic fluxes are integrated over the volume of NO production ($\dot{\omega}_{NO} > 0.1\,\mathrm{mol\,m^{-3}\ s^{-1}}$) and consumption ($\dot{\omega}_{NO} < -0.1\,\mathrm{mol\,m^{-3}\ s^{-1}}$) separately. The difference in NO emission predictions can be attributed to the respective formation pathways and production rates of NO in the Konnov and Stagni mechanisms. The reaction pathway via HNO dominates NO formation in

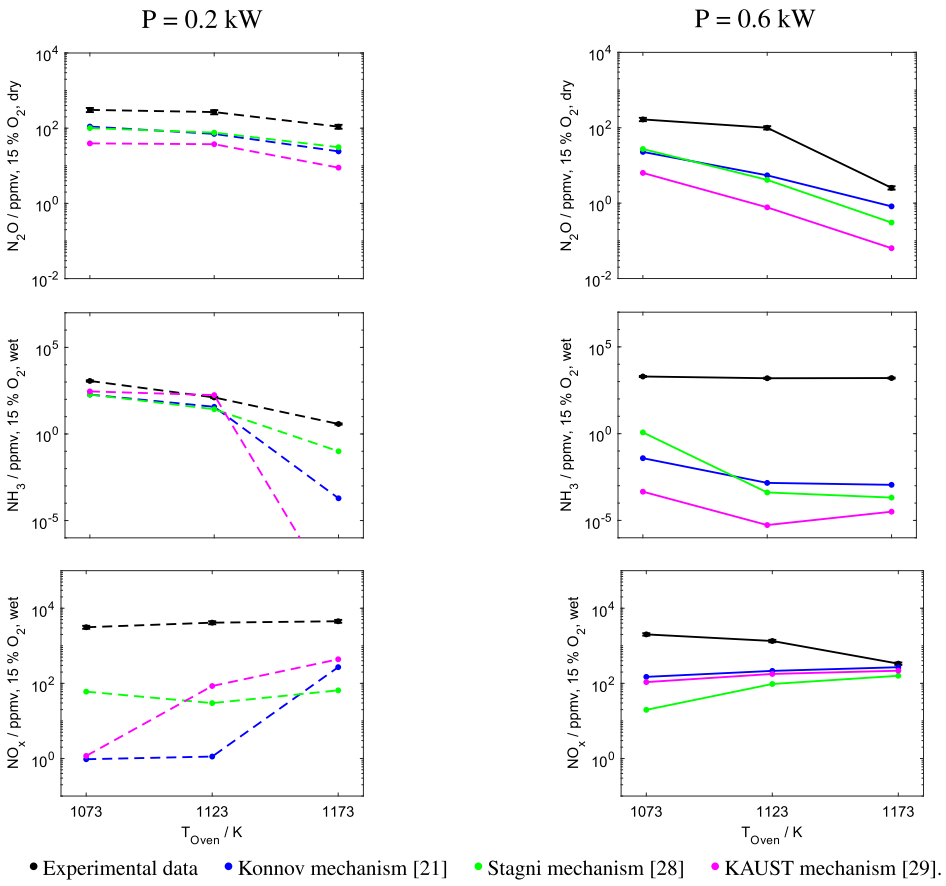

Fig. 6. Exhaust gas emissions at the burner outlet, normalized to 15 % O_2 following [23], are shown as a function of the nominal wall temperature for $P = 0.2$ kW (left) and $P = 0.6$ kW (right), based on experimental and predicted data from different reaction mechanisms (see legend for details). The NH_3 data at 0.2 kW and 1173 K computed using [29] is omitted, as it is five orders of magnitude below the scale.

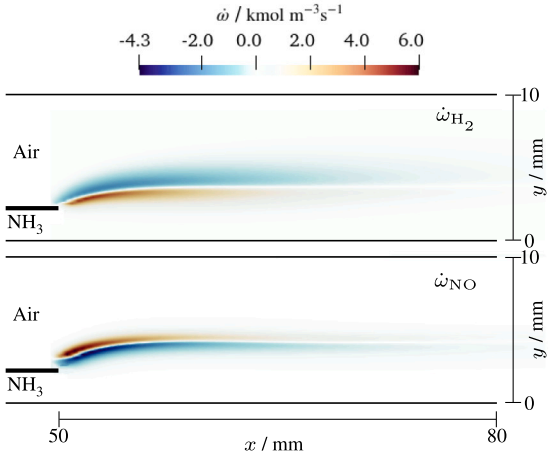

Fig. 7. H_2 and NO reaction rates for $P = 0.6$ kW and $T_{oven} = 1073$ K simulated with the Konnov mechanism.

both mechanisms. However, the reduction of NO_2 to NO has a higher flux in the Konnov mechanism, whereas the Zel'dovich reactions are more significant in the Stagni mechanism. In the NO consumption zone, pathways are comparable for both mechanisms, in terms of active paths and also their absolute fluxes. The global net production rates of NO, determined by integrating the reaction rates over the whole volume and normalizing by the total volume, from the Konnov and the Stagni mechanisms are 9.28×10^{-6} and 2.02×10^{-6} kmol $m^{-3}s^{-1}$, respectively. The lower global production rate of Stagni corroborates the predicted NO_x emissions for the selected conditions in Fig. 6.

4. Conclusion

In this study, laminar non-premixed ammonia flames were investigated both experimentally and numerically in a new slot burner design under varying preheating and wall temperatures, as well as thermal loads. The measurements included temperature data, spatially-resolved spectra, and global exhaust gas compositions of the major species and were compared with corresponding numerical data. The key findings are:

- The influence of thermal load and wall temperature on flame structure and the emissions of NO_x, NH_3, and N_2O in non-premixed combustion was investigated. The results show that flame length increases with thermal load, while the lowest emissions (335, 4, and 3 ppmv) were observed at high wall temperatures under varying thermal load. These findings provide valuable guidance for the development of low-emission ammonia combustion strategies.
- Spatially-resolved detection of OH*, NH*, and NH_2* was achieved using emission spectroscopy. Comparisons with numerical simulations showed strong agreement with the measured chemiluminescence in terms of shape and normalized intensity.
- Despite good agreement in intensity profiles, significant differences in emission characteristics remain. A key finding is the strong sensitivity of predicted emissions to the choice of reaction mechanism under strongly preheated conditions, highlighting the importance of mechanism selection and validation. Differences

are most pronounced in the NO production pathways. Additionally, imperfections in the experimental setup, violating the 2D assumptions and causing additional ammonia slip, may contribute to the observed deviations.
- The combination of experimental diagnostics and numerical simulations provides a deeper understanding of flame stabilization and chemical reaction mechanisms.

Novelty and significance statement

The novelty of this research is that non-premixed, laminar combustion of pure ammonia/air in a slot burner under well-defined conditions has not been studied before. In this study, major exhaust-gas species and emission spectra of non-premixed laminar ammonia flames are characterized, and commonly used ammonia reaction mechanisms are evaluated under these previously unexplored conditions. This research is significant because the combination of advanced experimental diagnostics and detailed numerical simulations provides new insights into chemical kinetics of non-premixed ammonia combustion. These findings provide valuable insights into the potential of non-premixed strategies for NO_x mitigation and the suitability of chemical reaction mechanisms, guiding future strategies for the sustainable utilization of ammonia as a carbon-free fuel.

CRediT authorship contribution statement

Daniel Kretzler: Writing – review & editing, Writing – original draft, Methodology, Investigation, Formal analysis. **Rishabh Puri:** Writing – review & editing, Software, Methodology, Investigation. **Björn Stelzner:** Writing – review & editing, Supervision, Conceptualization. **Thorsten Zirwes:** Writing – review & editing, Supervision, Conceptualization. **Fabian P. Hagen:** Writing – review & editing. **Oliver T. Stein:** Writing – review & editing, Supervision, Project administration, Funding acquisition. **Dimosthenis Trimis:** Writing – review & editing, Supervision, Project administration, Funding acquisition.

Declaration of competing interest

The authors declare that they have no known competing financial interests or personal relationships that could have appeared to influence the work reported in this paper.

Acknowledgments

The authors acknowledge the financial support by DFG, Germany (project number: 523876164, within PP2419 HyCAM). The authors also gratefully acknowledge the financial support by the Helmholtz Association of German Research Centers (HGF), within the research field Energy, program Materials and Technologies for the Energy Transition (MTET), topic Resource and Energy Efficiency, Anthropogenic Carbon Cycle (38.05.01).

Appendix A. Supplementary data

Supplementary material related to this article can be found online at https://doi.org/10.1016/j.proci.2025.105854.

References

[1] A. Valera-Medina, H. Xiao, M. Owen-Jones, W.I.F. David, P.J. Bowen, Ammonia for power, Prog. Energy Combust. Sci. 69 (2018) 63–102.
[2] Muhammad Aziz, Agung Tri Wijayanta, Asep Bayu Dani Nandiyanto, Ammonia as effective hydrogen storage: A review on production, storage and utilization, Energies 13 (12) (2020).
[3] Hideaki Kobayashi, Akihiro Hayakawa, K. Kunkuma A.D. Somarathne, Ekenechukwu C. Okafor, Science and technology of ammonia combustion, Proc. Combust. Inst. 37 (1) (2018) 109–133.
[4] J.H. Lee, J.H. Kim, J.H. Park, O.C. Kwon, Studies on properties of laminar premixed hydrogen-added ammonia/air flames for hydrogen production, Int. J. Hydrog. Energy 35 (3) (2010) 1054–1064.
[5] P. Forster, et al., The earth's energy budget, climate feedbacks, and climate sensitivity, climate change (2021): the physical science basis, in: Masson-Delmotte, et al. (Eds.), Contribution of Working Group I to the Sixth Assessment Report of the Intergovernmental Panel on Climate Change. V, Cambridge Univ. Press, 2021, pp. 923–1054.
[6] A. Valera-Medina, M.O. Vigueras-Zuniga, H. Shi, S. Mashruk, M. Alnajideen, A. Alnasif, J. Davies, Y. Wang, X. Zhu, W. Yang, Y.B. Cheng, Ammonia combustion in furnaces: A review, Int. J. Hydrog. Energy 49 (2024) 1597–1618.
[7] S. Mashruk, E.C. Okafor, M. Kovaleva, A. Alnasif, D. Pugh, A. Hayakawa, A. Valera-Medina, Evolution of N_2O production at lean combustion condition in NH_3/H_2/air premixed swirling flames, Combust. Flame 244 (2022) 112299.
[8] Ayman M. Elbaz, Shixing Wang, Thibault F. Guiberti, William L. Roberts, Review on the recent advances on ammonia combustion from the fundamentals to the applications, Fuel Commun. 10 (2022) 100053.
[9] Wai Siong Chai, Yulei Bao, Pengfei Jin, Guang Tang, Lei Zhou, A review on ammonia, ammonia-hydrogen and ammonia-methane fuels, Renew. Sustain. Energy Rev. 147 (2021).
[10] Siliang Ni, Dan Zhao, NO_x emission reduction in ammonia-powered micro-combustors by partially inserting porous medium under fuel-rich condition, Chem. Eng. J. 434 (2022).
[11] Fangyu Zhang, Gengxin Zhang, Zhongcheng Wang, Dawei Wu, Mehdi Jangi, Hongming Xu, Experimental investigation on combustion and emission characteristics of non-premixed ammonia/hydrogen flame, Int. J. Hydrog. Energy 61 (2024) 25–38.
[12] Yifeng Chen, Bin Zhang, Yi Su, Chunjie Sui, Junqing Zhang, Effect and mechanism of combustion enhancement and emission reduction for non-premixed pure ammonia combustion based on fuel preheating, Fuel 308 (2022).
[13] H. Yoshida, J.H. Yun, R. Echigo, T. Tomimura, Transient characteristics of combined conduction, convection and radiation heat transfer in porous media, Int. J. Heat Mass Transfer 33 (5) (1990) 847–857.
[14] D. Trimis, F. Durst, Combustion in a porous medium-advances and applications, Combust. Sci. Technol. 121 (1–6) (1996) 153–168.
[15] Christos Keramiotis, Björn Stelzner, Dimosthenis Trimis, Maria Founti, Porous burners for low emission combustion: An experimental investigation, Energy 45 (1) (2012) 213–219.
[16] Hadi Nozari, Onur Tuncer, Arif Karabeyoglu, Evaluation of ammonia-hydrogen-air combustion in SiC porous medium based burner, Energy Procedia 142 (2017) 674–679.
[17] Guillaume Vignat, Thorsten Zirwes, Edna R. Toro, Khaled Younes, Emeric Boigné, Priyanka Muhunthan, Lauren Simitz, Dimosthenis Trimis, Matthias Ihme, Experimental and numerical investigation of flame stabilization and pollutant formation in matrix stabilized ammonia-hydrogen combustion, Combust. Flame 250 (2023) 112642.
[18] Ryuichi Murai, Noriaki Nakatsuka, Hidetaka Higashino, Fumiteru Akamatsu, Review of fundamental study on ammonia direct combustion in industrial furnaces, in: CO2 Free Ammonia As an Energy Carrier, Japan's Insights, 2023, pp. 627–640.
[19] Gani Issayev, Xuren Zhu, Gianluca Capriolo, Thibault F. Guiberti, Spatially resolved NH* and OH* profiles in ammonia-hydrogen-air counterflow diffusion flames, Proc. Combust. Inst. 40 (1–4) (2024).
[20] Alexander A. Konnov, An exploratory modelling study of chemiluminescence in ammonia-fuelled flames. Part 1, Combust. Flame 253 (2023).
[21] Alexander A. Konnov, An exploratory modelling study of chemiluminescence in ammonia-fuelled flames. Part 2, Combust. Flame 253 (2023).
[22] Daniel Pugh, Jon Runyon, Philip Bowen, Anthony Giles, Agustin Valera-Medina, Richard Marsh, Burak Goktepe, Sally Hewlett, An investigation of ammonia primary flame combustor concepts for emissions reduction with OH*, NH_2* and NH* chemiluminescence at elevated conditions, Proc. Combust. Inst. 38 (4) (2021) 6451–6459.
[23] C.E. Baukal, P.B. Eleazer, Quantifying NOx for industrial combustion processes, J. Air Waste Manage. Assoc. 48 (1) (1998) 52–58.
[24] The mathworks inc, , in: MATLAB version: 9.13.0 (R2022a), Natick, Massachusetts, The MathWorks Inc., 2022, https://www.mathworks.com.
[25] Thorsten Zirwes, Marvin Sontheimer, Feichi Zhang, Abouelmagd Abdelsamie, Francisco E. Hernández Pérez, Oliver T. Stein, Hong G. Im, Andreas Kronenburg, Henning Bockhorn, Assessment of numerical accuracy and parallel performance of openfoam and its reacting flow extension ebIdnsFoam, Flow, Turbul. Combust. 111 (2) (2023) 567–602.
[26] David G. Goodwin, Harry K. Moffat, Ingmar Schoegl, Raymond L. Speth, Bryan W. Weber, Cantera: An object-oriented software toolkit for chemical kinetics, thermodynamics, and transport processes, 2023, Version 3.0.0.
[27] Robert J. Kee, Michael E. Coltrin, Peter Glarborg, Chemically reacting flow: theory and practice, John Wiley & Sons, 2005.

[28] Alessandro Stagni, Carlo Cavallotti, Suphaporn Arunthanayothin, Yu Song, Olivier Herbinet, Frédérique Battin-Leclerc, Tiziano Faravelli, An experimental, theoretical and kinetic-modeling study of the gas-phase oxidation of ammonia, React. Chem. Eng. 5 (2020) 696–711.

[29] X. Zhang, S.P. Moosakutty, P.R. Rajan, M. Younes, S.M. Sarathy, Combustion chemistry of ammonia/hydrogen mixtures: Jet-stirred reactor measurements and comprehensive kinetic modeling, Combust. Flame 234 (2021) 111653.

[30] Wubin Weng, Marcus Aldén, Zhongshan Li, Visible chemiluminescence of ammonia premixed flames and its application for flame diagnostics, Proc. Combust. Inst. 39 (4) (2023) 4327–4334.